

Double-strangeness hidden-charm pentaquarks

Samson Clymton,^{1,*} Hyun-Chul Kim,^{2,3,4,†} and Terry Mart^{5,‡}

¹*Asia Pacific Center for Theoretical Physics (APCTP), Pohang, Gyeongbuk 37673, Republic of Korea*

²*Department of Physics, Inha University, Incheon 22212, Republic of Korea*

³*Physics Research Institute, Inha University, Incheon 22212, Republic of Korea*

⁴*School of Physics, Korea Institute for Advanced Study (KIAS), Seoul 02455, Republic of Korea*

⁵*Departemen Fisika, FMIPA, Universitas Indonesia, Depok 16424, Indonesia*

(Dated: July 1, 2025)

We investigate the possible existence of double-strangeness hidden-charm pentaquark states, denoted as $P_{c\bar{c}s}$, within an off-shell coupled-channel formalism. Eleven meson–baryon channels with total strangeness $S = -2$ are constructed by combining charmed mesons and singly charmed baryons. The two-body scattering amplitudes are derived from an effective Lagrangian that respects heavy-quark spin symmetry, hidden local symmetry, and flavor SU(3) symmetry. The Bethe–Salpeter equation is solved using the Blankenbecler–Sugar reduction scheme, and resonances are identified as poles in the scattering amplitudes on the complex energy plane. We find five negative-parity $P_{c\bar{c}s}$ states with spins $J = 1/2, 3/2,$ and $5/2$, all located below their relevant thresholds. Three positive-parity states are also found: two with $J = 1/2$ and one with $J = 3/2$, lying above the thresholds with substantial widths. The coupling strengths of each resonance to relevant meson–baryon channels are extracted. The sensitivity of the results to the cutoff parameter $\Lambda_0 = \Lambda - m$ is examined. These results provide theoretical predictions that may assist future experimental searches for $P_{c\bar{c}s}$ states in the $J/\psi \Xi$ channel.

I. INTRODUCTION

The observation of hidden-charm pentaquark states [1–3] has generated significant experimental and theoretical interest in heavy pentaquark states (see the recent reviews [4–7] and references therein). Subsequently, the LHCb Collaboration reported the existence of a neutral hidden-charm pentaquark with strangeness, denoted as $P_{c\bar{c}s}(4459)$ [3, 8]. More recently, the Belle Collaboration confirmed the existence of $P_{c\bar{c}s}(4459)$ but reported a slightly larger mass, $M_{P_{c\bar{c}s}} = (4471.7 \pm 4.8 \pm 0.6) \text{ MeV}/c^2$, and a decay width of $\Gamma = (21.9 \pm 13.1 \pm 2.7) \text{ MeV}$ [9]. Given that the CMS and LHCb Collaborations have recently reported the decays $\Lambda_b^0 \rightarrow J/\psi \Xi^- K^+$ and $\Xi_b^0 \rightarrow J/\psi \Xi^- \pi^+$ [10, 11], the possible existence of hidden-charm pentaquark states with strangeness $S = -2$, denoted as $P_{c\bar{c}s}$, is anticipated. There have already been theoretical predictions for such double-strangeness hidden-charm pentaquarks [12–16].

In our previous work, we studied the production of hidden-charm pentaquark states with strangeness $S = 0$ and $S = -1$, using an off-shell coupled-channel approach to two-body charmed hadronic scattering [17, 18]. We first constructed the two-body kernel Feynman amplitudes for the relevant channels using an effective Lagrangian that respects heavy-quark spin–flavor symmetry, hidden local symmetry, and chiral symmetry. We then solved the coupled-channel scattering integral equations involving seven different channels for the non-strange $P_{c\bar{c}}$ states and nine different channels for the $P_{c\bar{c}s}$ states. The hidden-charm pentaquark states emerge as poles in the complex energy plane.

We found four hidden-charm pentaquark states with negative parity, which we associated with the $P_{c\bar{c}}$ states observed by the LHCb Collaboration: $P_{c\bar{c}}(4312)$, $P_{c\bar{c}}(4380)$, $P_{c\bar{c}}(4440)$, and $P_{c\bar{c}}(4457)$. In addition, we predicted the existence of two more negative-parity and two positive-parity $P_{c\bar{c}}$ states. We also explained the absence of a $P_{c\bar{c}}$ signal in the GlueX experiment for $J/\psi N$ photoproduction [19]: destructive interference in $J/\psi N$ scattering, combined with suppression due to dominant positive-parity contributions, weakens the hidden-charm pentaquark signals in the $J/\psi N$ channel [17]. Regarding the hidden-charm pentaquarks with $S = -1$, we identified seven $P_{c\bar{c}s}$ states with negative parity, among which $P_{c\bar{c}s}(4459)$, located below the $\bar{D}^* \Xi_c$ threshold, corresponds to the state observed by the LHCb Collaboration [3, 8]. Interestingly, we also found another state, $P_{c\bar{c}s}(4472)$, below the $\bar{D}^* \Xi_c$ threshold, whose mass matches that reported by the Belle Collaboration. Although this state has been considered identical to $P_{c\bar{c}s}(4459)$, it may in fact represent a separate resonance.

In the present work, we extend the off-shell coupled-channel formalism to study double-strangeness hidden-charm pentaquark states. Figure 1 summarizes the predictions for the $P_{c\bar{c}s}$ pentaquarks obtained in this study. We have found five resonances with negative parity and three with positive parity, covering spins $1/2, 3/2,$ and $5/2$. Notably,

* E-mail: samson.clymton@apctp.org

† E-mail: hchkim@inha.ac.kr

‡ E-mail: terry.mart@sci.ui.ac.id

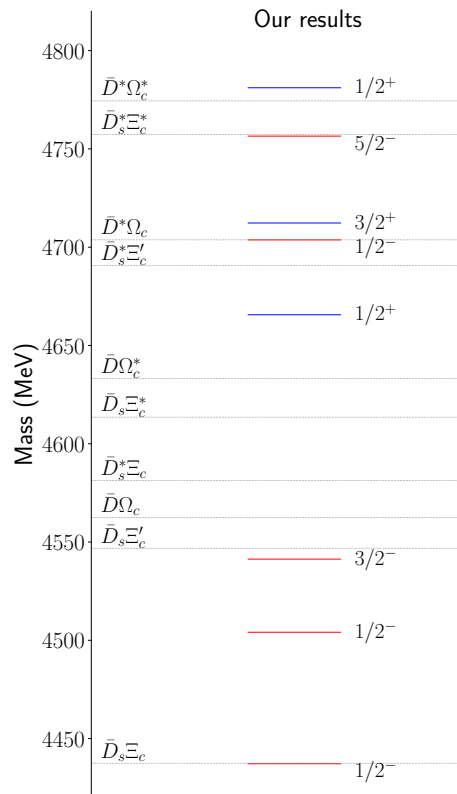


FIG. 1. Predicted $P_{c\bar{c}s}s$ states from the present work. Red lines denote double-strangeness hidden-charm pentaquark states with negative parity, whereas blue lines represent those with positive parity.

the negative-parity states lie below the corresponding thresholds, while the positive-parity ones are located above the thresholds.

The organization of the present work is as follows: In Sec. II, we describe the off-shell coupled-channel formalism. We begin by showing how the two-body kernel Feynman amplitudes are derived from an effective Lagrangian and proceed to solve the scattering integral equations. In Sec. III, we discuss the results for the double-strangeness hidden-charm pentaquarks. The final section is devoted to the summary and conclusions.

II. COUPLED-CHANNEL FORMALISM

The scattering amplitude can be expressed as

$$\mathcal{S}_{fi} = \delta_{fi} - i(2\pi)^4 \delta(P_f - P_i) \mathcal{T}_{fi}, \quad (1)$$

where P_i and P_f denote the total four-momenta of the initial and final states, respectively. The transition amplitudes \mathcal{T}_{fi} are obtained from the Bethe–Salpeter equation with the two-body Feynman kernel amplitudes:

$$\mathcal{T}_{fi}(p', p; s) = \mathcal{V}_{fi}(p', p; s) + \frac{1}{(2\pi)^4} \sum_k \int d^4q \mathcal{V}_{fk}(p', q; s) \mathcal{G}_k(q; s) \mathcal{T}_{ki}(q, p; s), \quad (2)$$

where p and p' are the relative four-momenta of the initial and final states, and q represents the off-shell momentum for intermediate states in the center-of-mass (CM) frame. The variable $s \equiv P_i^2 = P_f^2$ denotes the square of the total energy and corresponds to one of the Mandelstam variables. The indices i , f , and k refer to the initial, final, and intermediate states, respectively. Since we consider coupled channels relevant to the production of $P_{c\bar{c}s}s$ states, the index k runs over all relevant intermediate channels. The coupled integral scattering equations given in Eq. (2) are illustrated schematically in Fig. 2.

To simplify the challenges posed by the four-dimensional integral equations, we adopt a three-dimensional reduction approach. Among the various methods available, we employ the Blankenbecler–Sugar formalism [20, 21], which

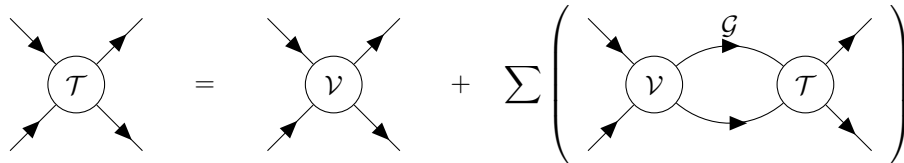


FIG. 2. Graphical representation of the coupled integral equation.

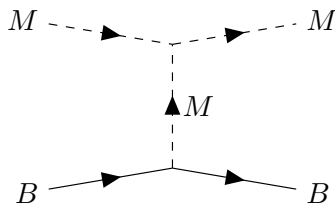
characterizes the two-body propagator as

$$\mathcal{G}_k(q) = \delta \left(q_0 - \frac{E_{k1}(\mathbf{q}) - E_{k2}(\mathbf{q})}{2} \right) \frac{\pi}{E_{k1}(\mathbf{q})E_{k2}(\mathbf{q})} \frac{E_k(\mathbf{q})}{s - E_k^2(\mathbf{q})}. \quad (3)$$

Here, E_k denotes the total on-shell energy of the intermediate state, defined as $E_k = E_{k1} + E_{k2}$, and \mathbf{q} represents the three-momentum of the intermediate state. It is important to note that the spinor contributions from the meson-baryon propagator G_k have been absorbed into the matrix elements of \mathcal{V} and \mathcal{T} . Using Eq. (3), we obtain the following coupled integral equations:

$$\mathcal{T}_{fi}(\mathbf{p}', \mathbf{p}) = \mathcal{V}_{fi}(\mathbf{p}', \mathbf{p}) + \frac{1}{(2\pi)^3} \sum_k \int \frac{d^3q}{2E_{k1}(\mathbf{q})E_{k2}(\mathbf{q})} \mathcal{V}_{fk}(\mathbf{p}', \mathbf{q}) \frac{E_k(\mathbf{q})}{s - E_k^2(\mathbf{q}) + i\varepsilon} \mathcal{T}_{ki}(\mathbf{q}, \mathbf{p}), \quad (4)$$

where \mathbf{p} and \mathbf{p}' denote the relative three-momenta of the initial and final states, respectively, in the CM frame.

FIG. 3. t -channel meson-exchange diagrams. M and B denote the meson and baryon, respectively.

To investigate the pentaquark $P_{c\bar{c}s}$'s, we construct two-body coupled channels by combining the charmed meson triplet with the singly charmed baryon antitriplet and sextet, while maintaining a total strangeness number of $S = -2$. We also include the $J/\psi\Xi$ channel, considering the fact that both the $P_{c\bar{c}}$ and $P_{c\bar{c}s}$ were observed in the invariant masses of $J/\psi N$ and $J/\psi\Lambda$, respectively. Thus, we include eleven distinct channels: $J/\psi\Xi$, $\bar{D}_s\Xi_c$, $\bar{D}_s\Xi'_c$, $\bar{D}\Omega_c$, $\bar{D}_s^*\Xi_c$, $\bar{D}_s\Xi_c^*$, $\bar{D}\Omega_c^*$, $\bar{D}_s^*\Xi'_c$, $\bar{D}^*\Omega_c$, $\bar{D}_s^*\Xi_c^*$, and $\bar{D}^*\Omega_c^*$. The two-body kernel Feynman amplitudes are constructed from tree-level one-meson-exchange diagrams, as illustrated in Fig. 3.

We exclude pole diagrams in the s -channel, since we want to see how the $P_{c\bar{c}s}$'s can be dynamically generated. The u -channel diagrams, which involve the exchange of doubly-charmed baryons with masses of approximately 3.5 GeV, are significantly suppressed in magnitude compared to the t -channel contributions and are thus also neglected in the present analysis.

We determine the vertex interactions using an effective Lagrangian that satisfies heavy-quark spin symmetry, hidden

local gauge symmetry, and flavor SU(3) symmetry [22], which are expressed as

$$\mathcal{L}_{PPV} = -i\frac{\beta g_V}{\sqrt{2}} P_a^\dagger \overleftrightarrow{\partial}_\mu P_b \mathbb{V}_{ba}^\mu + i\frac{\beta g_V}{\sqrt{2}} P_a'^\dagger \overleftrightarrow{\partial}_\mu P_b' \mathbb{V}_{ab}^\mu, \quad (5)$$

$$\mathcal{L}_{PP\sigma} = -2g_\sigma M P_a^\dagger \sigma P_a - 2g_\sigma M P_a'^\dagger \sigma P_a', \quad (6)$$

$$\mathcal{L}_{P^*P^*\mathbb{P}} = -\frac{g}{f_\pi} \epsilon^{\mu\nu\alpha\beta} P_{a\nu}^{*\dagger} \overleftrightarrow{\partial}_\mu P_{b\beta}^* \partial_\alpha \mathbb{P}_{ba} - \frac{g}{f_\pi} \epsilon^{\mu\nu\alpha\beta} P_{a\nu}'^{\dagger} \overleftrightarrow{\partial}_\mu P_{b\beta}'^* \partial_\alpha \mathbb{P}_{ab}, \quad (7)$$

$$\begin{aligned} \mathcal{L}_{P^*P^*\mathbb{V}} &= i\frac{\beta g_V}{\sqrt{2}} P_{a\nu}^{*\dagger} \overleftrightarrow{\partial}_\mu P_b^{*\nu} \mathbb{V}_{ba}^\mu + i2\sqrt{2}\lambda g_V M^* P_{a\mu}^{*\dagger} P_{b\nu}^* \mathbb{V}_{ba}^{\mu\nu} \\ &\quad - i\frac{\beta g_V}{\sqrt{2}} P_{a\nu}'^{\dagger} \overleftrightarrow{\partial}_\mu P_b'^{*\nu} \mathbb{V}_{ab}^\mu - i2\sqrt{2}\lambda g_V M^* P_{a\mu}'^{\dagger} P_{b\nu}'^* \mathbb{V}_{ab}^{\mu\nu}, \end{aligned} \quad (8)$$

$$\mathcal{L}_{P^*P^*\sigma} = 2g_\sigma M^* P_{a\mu}^{*\dagger} \sigma P_a^{*\mu} + 2g_\sigma M^* P_{a\mu}'^{\dagger} \sigma P_a'^{\mu}, \quad (9)$$

$$\mathcal{L}_{P^*P\mathbb{P}} = -\frac{2g}{f_\pi} \sqrt{MM^*} (P_a^\dagger P_{b\mu}^* + P_{a\mu}^{*\dagger} P_b) \partial^\mu \mathbb{P}_{ba} + \frac{2g}{f_\pi} \sqrt{MM^*} (P_a'^\dagger P_{b\mu}'^* + P_{a\mu}'^{\dagger} P_b') \partial^\mu \mathbb{P}_{ab}, \quad (10)$$

$$\begin{aligned} \mathcal{L}_{P^*P\mathbb{V}} &= -i\sqrt{2}\lambda g_V \epsilon^{\beta\alpha\mu\nu} \left(P_a^\dagger \overleftrightarrow{\partial}_\beta P_{b\alpha}^* + P_{a\alpha}^{*\dagger} \overleftrightarrow{\partial}_\beta P_b \right) (\partial_\mu \mathbb{V}_\nu)_{ba} \\ &\quad - i\sqrt{2}\lambda g_V \epsilon^{\beta\alpha\mu\nu} \left(P_a'^\dagger \overleftrightarrow{\partial}_\beta P_{b\alpha}'^* + P_{a\alpha}'^{\dagger} \overleftrightarrow{\partial}_\beta P_b' \right) (\partial_\mu \mathbb{V}_\nu)_{ab}, \end{aligned} \quad (11)$$

where $\overleftrightarrow{\partial} = \overrightarrow{\partial} - \overleftarrow{\partial}$. The σ stands for the lowest-lying isoscalar-scalar meson, f_0 . Heavy mesons and anti-heavy mesons $P^{(*)}$ and $P'^{(*)}$ are given as

$$P = (D^0, D^+, D_s^+), \quad P_\mu^* = (D_\mu^{*0}, D_\mu^{*+}, D_{s\mu}^{*+}), \quad P' = (\bar{D}^0, D^-, D_s^-), \quad P_\mu'^* = (\bar{D}_\mu'^{*0}, D_\mu'^{-}, D_{s\mu}'^{-}), \quad (12)$$

while the light pseudoscalar and vector mesons are written as

$$\mathbb{P} = \begin{pmatrix} \frac{1}{\sqrt{2}}\pi^0 + \frac{1}{\sqrt{6}}\eta & \pi^+ & K^+ \\ \pi^- & -\frac{1}{\sqrt{2}}\pi^0 + \frac{1}{\sqrt{6}}\eta & K^0 \\ K^- & \bar{K}^0 & -\frac{2}{\sqrt{6}}\eta \end{pmatrix}, \quad \mathbb{V}_\mu = \begin{pmatrix} \frac{1}{\sqrt{2}}\rho_\mu^0 + \frac{1}{\sqrt{2}}\omega_\mu & \rho_\mu^+ & K_\mu^{*+} \\ \rho_\mu^- & -\frac{1}{\sqrt{2}}\rho_\mu^0 + \frac{1}{\sqrt{2}}\omega_\mu & K_\mu^{*0} \\ K_\mu^{*-} & \bar{K}_\mu^{*0} & \phi_\mu \end{pmatrix}. \quad (13)$$

We determine the coupling constants in the Lagrangian as follows [23]: $g = 0.59 \pm 0.07 \pm 0.01$, which is established through experimental measurements of the full width for D^{*+} ; $g_V = m_\rho/f_\pi \approx 5.8$, which is derived by using the Kawarabayashi-Suzuki-Riazuddin-Fayyazuddin (KSUF) relation with $f_\pi = 132$ MeV; $\beta \approx 0.9$ [24, 25], which stems from the vector meson dominance in heavy meson radiative decay; and $\lambda = -0.56$ GeV $^{-1}$, which is extracted from light-cone sum rules and lattice QCD. It is important to note that the sign convention for λ differs from that in Ref. [23], as we utilize the same phase for heavy vector mesons found in Ref. [22]. For the sigma meson, the coupling constant is utilized to assess the 2π transition of $D_s(1^+)$ in Ref. [26]. The lowest isoscalar-scalar meson coupling is expressed as $g_\sigma = g_\pi/2\sqrt{6}$ with $g_\pi = 3.73$.

For the heavy baryon effective Lagrangian, we utilize the framework from Ref. [27], which incorporates a more comprehensive Lagrangian formulation as outlined in Ref. [28]. The baryonic interaction vertices within the tree-level

meson-exchange diagrams are characterized by the following effective Lagrangian:

$$\mathcal{L}_{B_3 B_3 \mathbb{V}} = \frac{i\beta_3 g_V}{2\sqrt{2}M_3} \left(\bar{B}_3 \overleftrightarrow{\partial}_\mu \mathbb{V}^\mu B_3 \right), \quad (14)$$

$$\mathcal{L}_{B_3 B_3 \sigma} = l_3 \left(\bar{B}_3 \sigma B_3 \right), \quad (15)$$

$$\mathcal{L}_{B_6 B_6 \mathbb{P}} = i \frac{g_1}{2f_\pi M_6} \bar{B}_6 \gamma_5 \left(\gamma^\alpha \gamma^\beta - g^{\alpha\beta} \right) \overleftrightarrow{\partial}_\alpha \partial_\beta \mathbb{P} B_6, \quad (16)$$

$$\mathcal{L}_{B_6 B_6 \mathbb{V}} = -i \frac{\beta_6 g_V}{2\sqrt{2}M_6} \left(\bar{B}_6 \overleftrightarrow{\partial}_\alpha \mathbb{V}^\alpha B_6 \right) - \frac{i\lambda_6 g_V}{3\sqrt{2}} \left(\bar{B}_6 \gamma_\mu \gamma_\nu \mathbb{V}^{\mu\nu} B_6 \right), \quad (17)$$

$$\mathcal{L}_{B_6 B_6 \sigma} = -l_6 \left(\bar{B}_6 \sigma B_6 \right), \quad (18)$$

$$\mathcal{L}_{B_6^* B_6^* \mathbb{P}} = \frac{3g_1}{4f_\pi M_6^*} \epsilon^{\mu\nu\alpha\beta} \left(\bar{B}_{6\mu}^* \overleftrightarrow{\partial}_\nu \partial_\alpha \mathbb{P} B_{6\beta}^* \right), \quad (19)$$

$$\mathcal{L}_{B_6^* B_6^* \mathbb{V}} = i \frac{\beta_6 g_V}{2\sqrt{2}M_6^*} \left(\bar{B}_{6\mu}^* \overleftrightarrow{\partial}_\alpha \mathbb{V}^\alpha B_{6\mu}^* \right) + \frac{i\lambda_6 g_V}{\sqrt{2}} \left(\bar{B}_{6\mu}^* \mathbb{V}^{\mu\nu} B_{6\nu}^* \right), \quad (20)$$

$$\mathcal{L}_{B_6^* B_6^* \sigma} = l_6 \left(\bar{B}_{6\mu}^* \sigma B_{6\mu}^* \right), \quad (21)$$

$$\mathcal{L}_{B_6 B_6^* \mathbb{P}} = \frac{g_1}{4f_\pi} \sqrt{\frac{3}{M_6^* M_6}} \epsilon^{\mu\nu\alpha\beta} \left[\left(\bar{B}_6 \gamma_5 \gamma_\mu \overleftrightarrow{\partial}_\nu \partial_\alpha \mathbb{P} B_{6\beta}^* \right) + \left(\bar{B}_{6\mu}^* \gamma_5 \gamma_\nu \overleftrightarrow{\partial}_\alpha \partial_\beta \mathbb{P} B_6 \right) \right], \quad (22)$$

$$\mathcal{L}_{B_6 B_6^* \mathbb{V}} = \frac{i\lambda_6 g_V}{\sqrt{6}} \left[\bar{B}_6 \gamma_5 \left(\gamma_\mu + \frac{i\overleftrightarrow{\partial}_\mu}{2\sqrt{M_6^* M_6}} \right) \mathbb{V}^{\mu\nu} B_{6\nu}^* + \bar{B}_{6\mu}^* \gamma_5 \left(\gamma_\nu - \frac{i\overleftrightarrow{\partial}_\nu}{2\sqrt{M_6^* M_6}} \right) \mathbb{V}^{\mu\nu} B_6 \right], \quad (23)$$

$$\mathcal{L}_{B_6 B_3 \mathbb{P}} = -\frac{g_4}{\sqrt{3}f_\pi} \left[\bar{B}_6 \gamma_5 \left(\gamma_\mu + \frac{i\overleftrightarrow{\partial}_\mu}{2\sqrt{M_6 M_3}} \right) \partial^\mu \mathbb{P} B_3 + \bar{B}_3 \gamma_5 \left(\gamma_\mu - \frac{i\overleftrightarrow{\partial}_\mu}{2\sqrt{M_6 M_3}} \right) \partial^\mu \mathbb{P} B_6 \right], \quad (24)$$

$$\mathcal{L}_{B_6 B_3 \mathbb{V}} = i \frac{\lambda_{63} g_V}{\sqrt{6}M_6 M_3} \epsilon^{\mu\nu\alpha\beta} \left[\left(\bar{B}_6 \gamma_5 \gamma_\mu \overleftrightarrow{\partial}_\nu \partial_\alpha \mathbb{V}_\beta B_3 \right) + \left(\bar{B}_3 \gamma_5 \gamma_\mu \overleftrightarrow{\partial}_\nu \partial_\alpha \mathbb{V}_\beta B_6 \right) \right], \quad (25)$$

$$\mathcal{L}_{B_6^* B_3 \mathbb{P}} = -\frac{g_4}{f_\pi} \left[\left(\bar{B}_{6\mu}^* \partial^\mu \mathbb{P} B_3 \right) + \left(\bar{B}_3 \partial^\mu \mathbb{P} B_{6\mu}^* \right) \right], \quad (26)$$

$$\mathcal{L}_{B_6^* B_3 \mathbb{V}} = i \frac{\lambda_{63} g_V}{\sqrt{2}M_6^* M_3} \epsilon^{\mu\nu\alpha\beta} \left[\left(\bar{B}_{6\mu}^* \overleftrightarrow{\partial}_\nu \partial_\alpha \mathbb{V}_\beta B_3 \right) + \left(\bar{B}_3 \overleftrightarrow{\partial}_\nu \partial_\alpha \mathbb{V}_\beta B_{6\mu}^* \right) \right], \quad (27)$$

with heavy baryon fields expressed as

$$B_3 = \begin{pmatrix} 0 & \Lambda_c^+ & \Xi_c^+ \\ -\Lambda_c^+ & 0 & \Xi_c^0 \\ -\Xi_c^+ & -\Xi_c^0 & 0 \end{pmatrix}, \quad B_6 = \begin{pmatrix} \Sigma_c^{++} & \frac{1}{\sqrt{2}}\Sigma_c^+ & \frac{1}{\sqrt{2}}\Xi_c^{\prime+} \\ \frac{1}{\sqrt{2}}\Sigma_c^+ & \Sigma_c^0 & \frac{1}{\sqrt{2}}\Xi_c^{\prime0} \\ \frac{1}{\sqrt{2}}\Xi_c^{\prime+} & \frac{1}{\sqrt{2}}\Xi_c^{\prime0} & \Omega_c^0 \end{pmatrix}, \quad B_6^* = \begin{pmatrix} \Sigma_c^{*++} & \frac{1}{\sqrt{2}}\Sigma_c^{*+} & \frac{1}{\sqrt{2}}\Xi_c^{*\prime+} \\ \frac{1}{\sqrt{2}}\Sigma_c^{*+} & \Sigma_c^{*0} & \frac{1}{\sqrt{2}}\Xi_c^{*\prime0} \\ \frac{1}{\sqrt{2}}\Xi_c^{*\prime+} & \frac{1}{\sqrt{2}}\Xi_c^{*\prime0} & \Omega_c^{*0} \end{pmatrix}. \quad (28)$$

The symbol B_μ denotes the spin 3/2 Rarita-Schwinger field, which is subject to the constraints

$$p^\mu B_\mu = 0 \quad \text{and} \quad \gamma^\mu B_\mu = 0. \quad (29)$$

Within this effective Lagrangian, the coupling constants are defined as follows [27, 29]: $\beta_3 = 6/g_V$, $\beta_6 = -2\beta_3$, $\lambda_6 = -3.31 \text{ GeV}^{-1}$, $\lambda_{63} = -\lambda_6/\sqrt{8}$, $g_1 = 0.942$ and $g_4 = 0.999$, $l_3 = -3.1$ and $l_6 = -2l_3$. The sign conventions we implement are in line with those established in Refs. [29, 30].

For hidden-charm channels, we concentrate solely on vector charmonia due to their immediate experimental significance. Nevertheless, including pseudoscalar charmonium states is straightforward, as we extend heavy quark spin symmetry principles to the charmonium domain as well [31]. The interaction between heavy mesons and charmonium is governed by the following effective Lagrangian [32]

$$\mathcal{L}_{PPJ/\psi} = -ig_\psi M \sqrt{m_J} \left(J/\psi^\mu P^\dagger \overleftrightarrow{\partial}_\mu P^{\prime\dagger} \right) + \text{h.c.}, \quad (30)$$

$$\mathcal{L}_{P^*PJ/\psi} = ig_\psi \sqrt{\frac{MM^*}{m_J}} \epsilon^{\mu\nu\alpha\beta} \partial_\mu J/\psi_\nu \left(P^\dagger \overleftrightarrow{\partial}_\alpha P^{*\prime\dagger} + P_\beta^{*\prime\dagger} \overleftrightarrow{\partial}_\alpha P^{\prime\dagger} \right) + \text{h.c.}, \quad (31)$$

$$\mathcal{L}_{P^*P^*J/\psi} = ig_\psi M^* \sqrt{m_J} (g^{\mu\nu} g^{\alpha\beta} - g^{\mu\alpha} g^{\nu\beta} + g^{\mu\beta} g^{\nu\alpha}) \left(J/\psi_\mu P_\nu^{*\prime\dagger} \overleftrightarrow{\partial}_\alpha P^{*\prime\dagger} \right) + \text{h.c.}. \quad (32)$$

Given the lack of experimental measurements for the $J/\psi \rightarrow D\bar{D}$ decay, Shimizu et al. [33] developed an estimation method for the coupling constant g_ψ : they initially calculated the coupling constant $g_{\phi K\bar{K}}$ from the experimental decay width of $\phi \rightarrow K\bar{K}$. Assuming that the J/ψ decay mechanisms parallel to those of the ϕ , with differences attributed mainly to mass variations, they derived an estimated coupling constant value of $g_\psi = 0.679 \text{ GeV}^{-3/2}$.

Following Ref. [33], we obtain the coupling constants between heavy baryons and heavy mesons as:

$$\mathcal{L}_{B_8 B_3 P} = g_{I\bar{3}} \sqrt{M} \bar{B}_8 \gamma_5 (P' B_3)_8 + \text{h.c.}, \quad (33)$$

$$\mathcal{L}_{B_8 B_3 P^*} = g_{I\bar{3}} \sqrt{M^*} \bar{B}_8 \gamma^\mu (P'_\mu B_3)_8 + \text{h.c.}, \quad (34)$$

$$\mathcal{L}_{B_8 B_6 P} = -g_{I6} \sqrt{3M} \bar{B}_8 \gamma_5 (P' B_6)_8 + \text{h.c.}, \quad (35)$$

$$\mathcal{L}_{B_8 B_6 P^*} = g_{I6} \sqrt{\frac{M^*}{3}} \bar{B}_8 \gamma^\mu (P'_\mu B_6)_8 + \text{h.c.}, \quad (36)$$

$$\mathcal{L}_{B_8 B_6^* P^*} = -2g_{I6} \sqrt{M^*} \bar{B}_8^\mu \gamma_5 (P'_\mu B_6)_8 + \text{h.c.} \quad (37)$$

The octet baryon matrix is expressed as

$$B_8 = \begin{pmatrix} \frac{1}{\sqrt{2}} \Sigma^0 + \frac{1}{\sqrt{6}} \Lambda & \Sigma^+ & p \\ \Sigma^- & -\frac{1}{\sqrt{2}} \Sigma^0 + \frac{1}{\sqrt{6}} \Lambda & n \\ \Xi^- & \Xi^0 & -\frac{2}{\sqrt{6}} \Lambda \end{pmatrix}, \quad (38)$$

while the octet components of the tensor product between triplet charmed meson and singly-heavy baryon are expressed as

$$(P' B_3)_8 = \begin{pmatrix} \frac{2}{3} \bar{D}^0 \Xi_c^0 + \frac{1}{3} D^- \Xi_c^+ - \frac{1}{3} D_s^- \Lambda_c^+ & -\bar{D}^0 \Xi_c^+ & \bar{D}^0 \Lambda_c^+ \\ D^- \Xi_c^0 & -\frac{2}{3} D^- \Xi_c^+ - \frac{1}{3} \bar{D}^0 \Xi_c^0 - \frac{1}{3} D_s^- \Lambda_c^+ & D^- \Lambda_c^+ \\ D_s^- \Xi_c^0 & -D_s^- \Xi_c^+ & \frac{2}{3} D_s^- \Lambda_c^+ - \frac{1}{3} \bar{D}^0 \Xi_c^0 + \frac{1}{3} D^- \Xi_c^+ \end{pmatrix}, \quad (39)$$

$$(P' B_6)_8 = \begin{pmatrix} \frac{1}{\sqrt{2}} (D_s^- \Sigma_c^+ - D^- \Xi_c'^+) & \frac{1}{\sqrt{2}} \bar{D}^0 \Xi_c'^+ - D_s^- \Sigma_c^{++} & D^- \Sigma_c^{++} - \frac{1}{\sqrt{2}} \bar{D}^0 \Sigma_c^+ \\ D_s^- \Sigma_c^0 - \frac{1}{\sqrt{2}} D^- \Xi_c'^0 & \frac{1}{\sqrt{2}} (\bar{D}^0 \Xi_c'^0 - D_s^- \Sigma_c^+) & \frac{1}{\sqrt{2}} D^- \Sigma_c^+ - \bar{D}^0 \Sigma_c^0 \\ \frac{1}{\sqrt{2}} D_s^- \Xi_c'^0 - D^- \Omega_c^0 & \bar{D}^0 \Omega_c^0 - \frac{1}{\sqrt{2}} D_s^- \Xi_c'^+ & \frac{1}{\sqrt{2}} (D^- \Xi_c'^+ - \bar{D}^0 \Xi_c'^0) \end{pmatrix}. \quad (40)$$

The structure is similar when we deal with charmed vector mesons or $J = 3/2$ sextet baryons. In this way, we have an SU(3) symmetric effective Lagrangian for the transition of singly heavy baryon to light baryon through charmed meson emission. From Ref. [33], we implement the coupling constants $g_{I\bar{3}} = -9.88 \text{ GeV}^{-1/2}$ and $g_{I6} = 1.14 \text{ GeV}^{-1/2}$. It is worth noting that the coupling to hidden-charm channels plays only a minor role in the resonance production mechanism. The predicted masses of hidden-charm pentaquarks show little variation with changes in these coupling constants.

The Feynman amplitude for a one-meson exchange diagram can be expressed as

$$\mathcal{A}_{\lambda'_1 \lambda'_2, \lambda_1 \lambda_2} = \text{IS} F^2(q^2) \Gamma_{\lambda'_1 \lambda'_2}(p'_1, p'_2) \mathcal{P}(q) \Gamma_{\lambda_1 \lambda_2}(p_1, p_2), \quad (41)$$

where λ_i and p_i denote respectively the helicity and momentum of each particle participating in the process, while q designates the momentum transfer. The IS factor contains the SU(3) Clebsch-Gordan coefficient and isospin factor, with values for each exchange diagram documented in Table I. We derive the vertex Γ from the effective Lagrangian, and express the propagators for spin-0 and spin-1 mesons as

$$\mathcal{P}(q) = \frac{1}{q^2 - m^2}, \quad \mathcal{P}_{\mu\nu}(q) = \frac{1}{q^2 - m^2} \left(-g_{\mu\nu} + \frac{q_\mu q_\nu}{m^2} \right). \quad (42)$$

For the heavy-meson propagators, we adopt the same form as for the light mesons, since the heavy-quark mass is finite.

Since hadrons have finite hadron sizes, we need to introduce a form factor at each vertex. We employ the following form of the form factor [34]

$$F(q^2) = \left(\frac{n\Lambda^2 - m^2}{n\Lambda^2 - q^2} \right)^n, \quad (43)$$

TABLE I. Values of the IS factors for the corresponding t -channel diagrams for the given reactions.

Reactions	Exchange particles	IS
$J/\psi\Xi \rightarrow \bar{D}_s\Xi_c$	\bar{D}_s, \bar{D}_s^*	-1
$J/\psi\Xi \rightarrow \bar{D}_s\Xi'_c$	\bar{D}_s, \bar{D}_s^*	$\frac{1}{2}\sqrt{2}$
$J/\psi\Xi \rightarrow \bar{D}\Omega_c$	\bar{D}, \bar{D}^*	-1
$J/\psi\Xi \rightarrow \bar{D}_s^*\Xi_c$	\bar{D}_s, \bar{D}_s^*	-1
$J/\psi\Xi \rightarrow \bar{D}_s\Xi_c^*$	\bar{D}_s, \bar{D}_s^*	$\frac{1}{2}\sqrt{2}$
$J/\psi\Xi \rightarrow \bar{D}\Omega_c^*$	\bar{D}, \bar{D}^*	-1
$J/\psi\Xi \rightarrow \bar{D}_s^*\Xi'_c$	\bar{D}_s, \bar{D}_s^*	$\frac{1}{2}\sqrt{2}$
$J/\psi\Xi \rightarrow \bar{D}^*\Omega_c$	\bar{D}, \bar{D}^*	-1
$J/\psi\Xi \rightarrow \bar{D}_s^*\Xi_c^*$	\bar{D}_s, \bar{D}_s^*	$\frac{1}{2}\sqrt{2}$
$J/\psi\Xi \rightarrow \bar{D}^*\Omega_c^*$	\bar{D}, \bar{D}^*	-1
$\bar{D}_s\Xi_c \rightarrow \bar{D}_s\Xi_c$	ϕ	1
	σ	2
$\bar{D}_s\Xi_c \rightarrow \bar{D}_s\Xi'_c$	ϕ	$-\frac{1}{2}\sqrt{2}$
$\bar{D}_s\Xi_c \rightarrow \bar{D}\Omega_c$	K^*	1
$\bar{D}_s\Xi_c \rightarrow \bar{D}_s^*\Xi_c$	ϕ	1
$\bar{D}_s\Xi_c \rightarrow \bar{D}_s\Xi_c^*$	ϕ	$-\frac{1}{2}\sqrt{2}$
$\bar{D}_s\Xi_c \rightarrow \bar{D}\Omega_c^*$	K^*	1
$\bar{D}_s\Xi_c \rightarrow \bar{D}_s^*\Xi'_c$	η	$-\frac{1}{2}\sqrt{2}$
	ϕ	$-\frac{1}{2}\sqrt{2}$
$\bar{D}_s\Xi_c \rightarrow \bar{D}^*\Omega_c$	K, K^*	1
$\bar{D}_s\Xi_c \rightarrow \bar{D}_s^*\Xi_c^*$	η	$-\frac{1}{2}\sqrt{2}$
	ϕ	$-\frac{1}{2}\sqrt{2}$
$\bar{D}_s\Xi_c \rightarrow \bar{D}^*\Omega_c^*$	K, K^*	1
$\bar{D}_s\Xi'_c \rightarrow \bar{D}_s\Xi'_c$	ϕ	$\frac{1}{2}$
	σ	1
$\bar{D}_s\Xi'_c \rightarrow \bar{D}\Omega_c$	K^*	$\frac{1}{2}\sqrt{2}$
$\bar{D}_s\Xi'_c \rightarrow \bar{D}_s^*\Xi_c$	η	$-\frac{1}{2}\sqrt{2}$
	ϕ	$-\frac{1}{2}\sqrt{2}$
$\bar{D}_s\Xi'_c \rightarrow \bar{D}_s\Xi_c^*$	ϕ	$\frac{1}{2}$
$\bar{D}_s\Xi'_c \rightarrow \bar{D}\Omega_c^*$	K^*	$\frac{1}{2}\sqrt{2}$
$\bar{D}_s\Xi'_c \rightarrow \bar{D}_s^*\Xi'_c$	η	$\frac{1}{6}$
	ϕ	$\frac{1}{2}$
$\bar{D}_s\Xi'_c \rightarrow \bar{D}^*\Omega_c$	K, K^*	$\frac{1}{2}\sqrt{2}$
$\bar{D}_s\Xi'_c \rightarrow \bar{D}_s^*\Xi_c^*$	η	$\frac{1}{6}$
	ϕ	$\frac{1}{2}$
$\bar{D}_s\Xi'_c \rightarrow \bar{D}^*\Omega_c^*$	K, K^*	$\frac{1}{2}\sqrt{2}$
$\bar{D}\Omega_c \rightarrow \bar{D}\Omega_c$	σ	1
$\bar{D}\Omega_c \rightarrow \bar{D}_s^*\Xi_c$	\bar{K}, \bar{K}^*	1
$\bar{D}\Omega_c \rightarrow \bar{D}_s\Xi_c^*$	\bar{K}^*	$\frac{1}{2}\sqrt{2}$
$\bar{D}\Omega_c \rightarrow \bar{D}_s^*\Xi'_c$	\bar{K}, \bar{K}^*	$\frac{1}{2}\sqrt{2}$
$\bar{D}\Omega_c \rightarrow \bar{D}^*\Omega_c$	η	$-\frac{1}{6}\sqrt{2}$
$\bar{D}\Omega_c \rightarrow \bar{D}_s^*\Xi_c^*$	\bar{K}, \bar{K}^*	$\frac{1}{2}\sqrt{2}$
$\bar{D}\Omega_c \rightarrow \bar{D}^*\Omega_c^*$	η	$-\frac{1}{6}\sqrt{2}$

TABLE I. Values of the IS factors for the corresponding t -channel diagrams for the given reactions (continued).

Reactions	Exchange particles	IS
$\bar{D}_s^* \Xi_c \rightarrow \bar{D}_s^* \Xi_c$	ϕ	1
	σ	2
$\bar{D}_s^* \Xi_c \rightarrow \bar{D}_s \Xi_c^*$	η	$-\frac{1}{2}\sqrt{2}$
	ϕ	$-\frac{1}{2}\sqrt{2}$
$\bar{D}_s^* \Xi_c \rightarrow \bar{D} \Omega_c^*$	K, K^*	1
$\bar{D}_s^* \Xi_c \rightarrow \bar{D}_s^* \Xi_c'$	η	$-\frac{1}{2}\sqrt{2}$
	ϕ	$-\frac{1}{2}\sqrt{2}$
$\bar{D}_s^* \Xi_c \rightarrow \bar{D}^* \Omega_c$	K, K^*	1
$\bar{D}_s^* \Xi_c \rightarrow \bar{D}_s^* \Xi_c^*$	η	$-\frac{1}{2}\sqrt{2}$
	ϕ	$-\frac{1}{2}\sqrt{2}$
$\bar{D}_s \Xi_c \rightarrow \bar{D}^* \Omega_c^*$	K, K^*	1
$\bar{D}_s \Xi_c \rightarrow \bar{D}_s \Xi_c^*$	ϕ	$\frac{1}{2}$
	σ	1
$\bar{D}_s \Xi_c^* \rightarrow \bar{D} \Omega_c^*$	K^*	$\frac{1}{2}\sqrt{2}$
$\bar{D}_s \Xi_c^* \rightarrow \bar{D}_s^* \Xi_c'$	η	$\frac{1}{6}$
	ϕ	$\frac{1}{2}$
$\bar{D}_s \Xi_c^* \rightarrow \bar{D}^* \Omega_c$	K, K^*	$\frac{1}{2}\sqrt{2}$
$\bar{D}_s \Xi_c^* \rightarrow \bar{D}_s^* \Xi_c^*$	η	$\frac{1}{6}$
	ϕ	$\frac{1}{2}$
$\bar{D}_s \Xi_c^* \rightarrow \bar{D}^* \Omega_c^*$	K, K^*	$\frac{1}{2}\sqrt{2}$
$\bar{D} \Omega_c^* \rightarrow \bar{D} \Omega_c^*$	σ	1
$\bar{D} \Omega_c^* \rightarrow \bar{D}_s^* \Xi_c'$	\bar{K}, \bar{K}^*	$\frac{1}{2}\sqrt{2}$
$\bar{D} \Omega_c^* \rightarrow \bar{D}^* \Omega_c$	η	$-\frac{1}{6}\sqrt{2}$
$\bar{D} \Omega_c^* \rightarrow \bar{D}_s^* \Xi_c^*$	\bar{K}, \bar{K}^*	$\frac{1}{2}\sqrt{2}$
$\bar{D} \Omega_c^* \rightarrow \bar{D}^* \Omega_c^*$	η	$-\frac{1}{6}\sqrt{2}$
$\bar{D}_s^* \Xi_c' \rightarrow \bar{D}_s^* \Xi_c'$	η	$\frac{1}{6}$
	ϕ	$\frac{1}{2}$
	σ	1
$\bar{D}_s^* \Xi_c' \rightarrow \bar{D}^* \Omega_c$	K, K^*	$\frac{1}{2}\sqrt{2}$
$\bar{D}_s^* \Xi_c' \rightarrow \bar{D}_s^* \Xi_c^*$	η	$\frac{1}{6}$
	ϕ	$\frac{1}{2}$
$\bar{D}_s^* \Xi_c' \rightarrow \bar{D}^* \Omega_c^*$	K, K^*	$\frac{1}{2}\sqrt{2}$
$\bar{D}^* \Omega_c \rightarrow \bar{D}^* \Omega_c$	η	$-\frac{1}{6}\sqrt{2}$
	σ	1
$\bar{D}^* \Omega_c \rightarrow \bar{D}_s^* \Xi_c^*$	\bar{K}, \bar{K}^*	$\frac{1}{2}\sqrt{2}$
$\bar{D}^* \Omega_c \rightarrow \bar{D}^* \Omega_c^*$	η	$-\frac{1}{6}\sqrt{2}$
$\bar{D}_s^* \Xi_c^* \rightarrow \bar{D}_s^* \Xi_c^*$	η	$\frac{1}{6}$
	ϕ	$\frac{1}{2}$
	σ	1
$\bar{D}_s^* \Xi_c^* \rightarrow \bar{D}^* \Omega_c^*$	K, K^*	$\frac{1}{2}\sqrt{2}$
$\bar{D}^* \Omega_c^* \rightarrow \bar{D}^* \Omega_c^*$	η	$-\frac{1}{6}\sqrt{2}$
	σ	1

where the value of n depends on the momentum power present in the vertex. A key benefit of this parametrization is that modifying Λ becomes unnecessary when n changes. It should be observed that as n approaches infinity, Eq. (43) transforms into a Gaussian form. While it is difficult to determine the cutoff masses Λ in Eq. (43) on account of a lack of experimental information, we utilize a physical feature of hadron sizes to reduce the uncertainties due to the cutoff masses. Previous studies indicate that heavy hadrons exhibit more compact sizes than their lighter counterparts [35, 36], suggesting that higher cutoff masses are appropriate for heavy hadrons compared to light hadrons. Based on this reasoning, we define a value of the reduced cutoff mass as $\Lambda_0 := \Lambda - m$, where m corresponds to the mass of the exchange particle. In the absence of experimental data on the $P_{c\bar{c}s}s$, we apply a consistent value of 700 MeV across all reduced cutoff parameters Λ_0 .

In the context of the strong interaction, we can use parity invariance to reduce the number of independent amplitudes required. The parity relation is mathematically formulated as:

$$\mathcal{A}_{-\lambda'_1-\lambda'_2, -\lambda_1-\lambda_2} = \eta(\eta')^{-1} \mathcal{A}_{\lambda'_1\lambda'_2, \lambda_1\lambda_2}, \quad (44)$$

with η and η' defined by:

$$\eta = \eta_1\eta_2(-1)^{J-s_1-s_2}, \quad \eta' = \eta'_1\eta'_2(-1)^{J-s'_1-s'_2}. \quad (45)$$

In these expressions, η_i and s_i represent the intrinsic parity and spin of the particle respectively, while J corresponds to the total angular momentum. This relationship significantly decreases the computational time required for numerical calculations.

To enhance computational efficiency and elucidate the spin-parity classifications of $P_{c\bar{c}s}s$ states, we implement a partial-wave decomposition of the \mathcal{V} and \mathcal{T} matrices. This approach yields a simplified one-dimensional integral equation:

$$\mathcal{T}_{\lambda'\lambda}^{J(fi)}(\mathbf{p}', \mathbf{p}) = \mathcal{V}_{\lambda'\lambda}^{J(fi)}(\mathbf{p}', \mathbf{p}) + \frac{1}{(2\pi)^3} \sum_{k, \lambda_k} \int \frac{q^2 dq}{2E_{k1}E_{k2}} \mathcal{V}_{\lambda'\lambda_k}^{J(fk)}(\mathbf{p}', \mathbf{q}) \frac{E_k}{s - E_k^2 + i\epsilon} \mathcal{T}_{\lambda_k\lambda}^{J(ki)}(\mathbf{q}, \mathbf{p}), \quad (46)$$

where the helicities of the final, initial, and intermediate states are denoted by $\lambda' = \{\lambda'_1, \lambda'_2\}$, $\lambda = \{\lambda_1, \lambda_2\}$, and $\lambda_k = \{\lambda_{k1}, \lambda_{k2}\}$, respectively. The variables \mathbf{p}' , \mathbf{p} , and \mathbf{q} correspond to the magnitudes of the momentum vectors \mathbf{p}' , \mathbf{p} , and \mathbf{q} . We express the partial-wave kernel amplitudes $\mathcal{V}_{\lambda'\lambda}^{J(fi)}$ as

$$\mathcal{V}_{\lambda'\lambda}^{J(fi)}(\mathbf{p}', \mathbf{p}) = 2\pi \int d(\cos\theta) d_{\lambda_1-\lambda_2, \lambda'_1-\lambda'_2}^J(\theta) \mathcal{V}_{\lambda'\lambda}^{fi}(\mathbf{p}', \mathbf{p}, \theta), \quad (47)$$

where θ represents the scattering angle and $d_{\lambda\lambda'}^J(\theta)$ refers to the reduced Wigner D functions.

The integral equation presented in Eq. (46) contains a singularity coming from the two-body propagator \mathcal{G} . To effectively manage this singularity, we treat its singular component independently. The resulting regularized integral equation takes the form:

$$\mathcal{T}_{\lambda'\lambda}^{fi}(\mathbf{p}', \mathbf{p}) = \mathcal{V}_{\lambda'\lambda}^{fi}(\mathbf{p}', \mathbf{p}) + \frac{1}{(2\pi)^3} \sum_{k, \lambda_k} \left[\int_0^\infty dq \frac{qE_k}{E_{k1}E_{k2}} \frac{\mathcal{F}(q) - \mathcal{F}(\tilde{q}_k)}{s - E_k^2} + \frac{1}{2\sqrt{s}} \left(\ln \left| \frac{\sqrt{s} - E_k^{\text{thr}}}{\sqrt{s} + E_k^{\text{thr}}} \right| - i\pi \right) \mathcal{F}(\tilde{q}_k) \right], \quad (48)$$

where

$$\mathcal{F}(q) = \frac{1}{2} q \mathcal{V}_{\lambda'\lambda_k}^{fk}(\mathbf{p}', \mathbf{q}) \mathcal{T}_{\lambda_k\lambda}^{ki}(\mathbf{q}, \mathbf{p}), \quad (49)$$

and \tilde{q}_k represents the momentum q when $E_{k1} + E_{k2} = \sqrt{s}$. This regularization procedure is implemented exclusively when the total energy \sqrt{s} is greater than the threshold energy of the k -th channel E_k^{thr} . Notably, the form factors incorporated in the kernel amplitudes \mathcal{V} guarantee the unitarity of the transition amplitudes in the high-momentum domain.

For the numerical evaluation of the \mathcal{T} matrix in Eq. (48), we decompose the \mathcal{V} matrix in the helicity basis and represent it in momentum space, with momenta determined via the Gaussian quadrature method. The \mathcal{T} matrix is subsequently derived through the Haftel–Tabakin matrix inversion technique [37]:

$$\mathcal{T} = \left(1 - \mathcal{V}\tilde{\mathcal{G}}\right)^{-1} \mathcal{V}. \quad (50)$$

The derived \mathcal{T} matrix, expressed in the helicity basis, lacks definite parity. To investigate the parity classifications of the $P_{c\bar{c}s}s$ states, we transform the transition amplitudes into partial-wave amplitudes with well-defined parity:

$$\mathcal{T}_{\lambda'\lambda}^{J\pm} = \frac{1}{2} \left[\mathcal{T}_{\lambda'\lambda}^J \pm \eta_1 \eta_2 (-1)^{s_1+s_2+\frac{1}{2}} \mathcal{T}_{\lambda'-\lambda}^J \right], \quad (51)$$

where $\mathcal{T}^{J\pm}$ represents the partial-wave transition amplitude with total angular momentum J and parity $(-1)^{J\pm 1/2}$. The coefficient 1/2 ensures that no additional scaling factor is required when reverting to the partial-wave component:

$$\mathcal{T}_{\lambda'\lambda}^J = \mathcal{T}_{\lambda'\lambda}^{J+} + \mathcal{T}_{\lambda'\lambda}^{J-}. \quad (52)$$

It is important to note that decomposing the partial-wave component with definite parity in Eq. (46) is superfluous, as parity invariance is already integrated into both the effective Lagrangian and the amplitude calculations, as demonstrated in Eq. (44).

For our analysis of dynamically generated resonances, we reformulate the \mathcal{T} matrix in the IJL particle basis [38]. The transformational relationships between the \mathcal{T} matrix elements across these two bases are expressed as:

$$\mathcal{T}_{L'L}^{JS'S'} = \frac{\sqrt{(2L+1)(2L'+1)}}{2J+1} \sum_{\lambda'_1 \lambda'_2 \lambda_1 \lambda_2} (L'0S'\lambda'|J\lambda') (s'_1 \lambda'_1 s'_2 - \lambda'_2 |S'\lambda') (L0S\lambda|J\lambda) (s_1 \lambda_1 s_2 - \lambda_2 |S\lambda) \mathcal{T}_{\lambda'_1 \lambda'_2 \lambda_1 \lambda_2}^J. \quad (53)$$

In the present study, we focus exclusively on the diagonal component \mathcal{T}_L^{JS} , as it has the most significant implications for the production of the double-strangeness hidden-charm pentaquarks.

III. RESULTS AND DISCUSSIONS

As mentioned previously, we have introduced the eleven different channels to investigate the dynamical generation of the double-strangeness hidden-charm pentaquark states. It implies that we also have eleven different two-particle thresholds: $J/\psi\Xi$, $\bar{D}_s\Xi_c$, $\bar{D}_s\Xi'_c$, $\bar{D}\Omega_c$, $\bar{D}_s^*\Xi_c$, $\bar{D}_s\Xi_c^*$, $\bar{D}\Omega_c^*$, $\bar{D}_s^*\Xi'_c$, $\bar{D}^*\Omega_c$, $\bar{D}_s^*\Xi_c^*$, and $\bar{D}^*\Omega_c^*$ in the order of increasing the threshold energies. In the previous works on the hidden-charm pentaquark states with $S = 0$ [17] and $S = -1$ [18], those with negative parity were always located below the thresholds, whereas those with positive parity were found above the thresholds. As will be shown in this work, we will see the same tendency in the case of the double-strangeness hidden-charm pentaquarks. We limit our discussion to the cases where total isospin equals 1/2, anticipating that the $P_{c\bar{c}s}s$ may be observed in the $J/\psi\Xi$ invariant mass distributions. Since experimental data are not yet available, we will focus on finding most probable pole position of the $P_{c\bar{c}s}s$ resonances. Table I lists all the parameters used in the exchange diagram to generate the kernel Feynman amplitudes. Regarding theoretical uncertainties arising from the cutoff masses, we will discuss it at the end of this section.

A. Negative parity

Figure 4 draws the results for the $i \rightarrow J/\psi\Xi$ transition partial-wave cross sections for the total angular momentum $J = 1/2, 3/2, 5/2$ with negative parity, which correspond to the spins and parity of $P_{c\bar{c}s}s$, as functions of the total energy. i represents the initial two-particle states, as expressed in the legend of Fig. 4. As shown in the upper-left panel of Fig. 4, we identify three resonances with spin-parity $J^P = 1/2^-$. On the other hand, the upper-right panel and lower panel of Fig. 4 demonstrate a resonance with $J^P = 3/2^-$ and that with $J^P = 5/2^-$, respectively. Table II lists the pole positions of these five negative-parity pentaquark resonances in the complex plane, and numerical results for the coupling strengths to the coupled channels involved.

The first resonance is located almost at the $\bar{D}_s\Xi_c$ threshold. Its pole position is determined to be $M_{P_{c\bar{c}s}s} - i\Gamma/2 = (4437.2 - i0.002)$ MeV. Interestingly, the width is tiny, which indicates that the $P_{c\bar{c}s}s(4437)$ is almost stable. Since the $J/\psi\Xi$ threshold lies lower than this resonance, it decays into J/ψ and Ξ . Table II shows that the most dominant contribution to the first resonance come from the $\bar{D}_s\Xi_c(^2S_{1/2})$ channel. The next most dominant one is the $\bar{D}^*\Omega_c(^2S_{1/2})$ channel. The $\bar{D}^*\Omega_c(^2S_{1/2})$, $\bar{D}_s^*\Xi'_c(^2S_{1/2})$, and $\bar{D}_s^*\Xi_c(^2S_{1/2})$ channels also come into significant play. Note that the D -wave contributions are small. It is interesting to see that the $\bar{D}^*\Omega_c(^2S_{1/2})$ channel is large, even though the corresponding threshold energy ($E_{\text{th}} = 4774$ MeV) is quite higher than the mass of the $P_{c\bar{c}s}s(4437)$. Actually, the transition amplitude for the $\bar{D}_s\Xi_c \rightarrow \bar{D}^*\Omega_c$ process is larger than that for the $\bar{D}_s\Xi_c \rightarrow \bar{D}\Omega_c$ transition. The reason is that while both K - and K^* -exchange are involved in the $\bar{D}_s\Xi_c \rightarrow \bar{D}^*\Omega_c$ transition, only K^* -exchange enters in

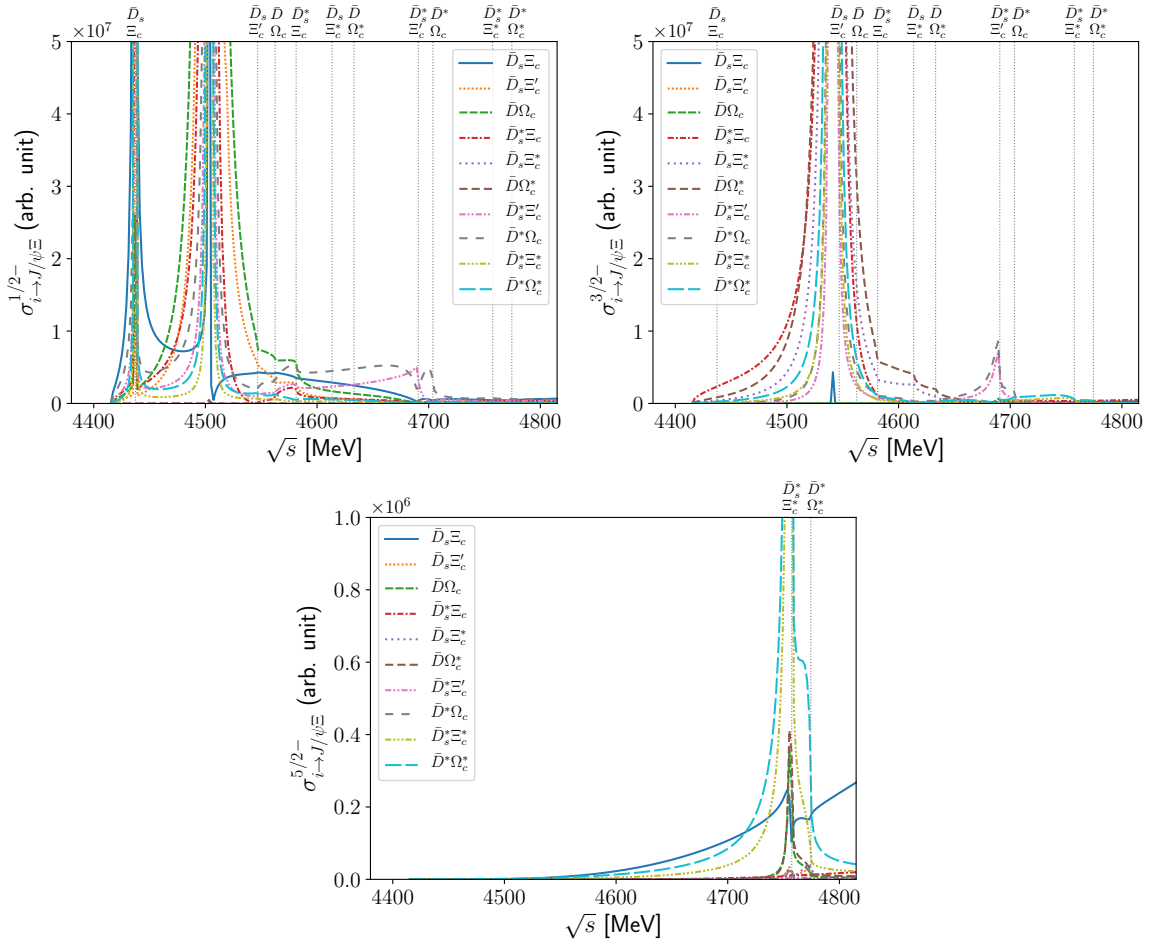


FIG. 4. $i \rightarrow J/\psi \Xi$ transition partial-wave cross sections for the given total angular momenta $J = 1/2, 3/2, 5/2$ with negative parity, which correspond to the spins and parity of $P_{c\bar{c}s s}$, as functions of the total energy. i denotes the initial two-particle states, as expressed in the legend.

the $\bar{D}_s \Xi_c \rightarrow \bar{D} \Omega_c$. It also implies that K -exchange is more significant than K^* -exchange. The difference between the $\bar{D}^* \Omega_c ({}^2S_{1/2})$ and $\bar{D}_s^* \Xi_c ({}^2S_{1/2})$ channels is related to the different values of the IS factor, as shown in Table I. Having examined the coupling strengths of the $P_{c\bar{c}s s}(4437)$ resonance to each channel, we draw a conclusion that it is not a specific meson-baryon molecular state, because the four different channels mentioned above are of the similar strengths. This is a distinguished feature from the cases of the $P_{c\bar{c}}$ and $P_{c\bar{c}s}$ resonances discussed in Refs. [17, 18].

The pole position of the second resonance with $J^P = 1/2^-$ is obtained to be $M_{P_{c\bar{c}s s}} - i\Gamma/2 = (4504.1 - i0.2)$ MeV, which lies between the $\bar{D}_s \Xi_c$ and $\bar{D}_s \Xi_c'$ thresholds. Table II shows three channels most dominantly contribute to this resonance in the following order: $\bar{D} \Omega_c$, $\bar{D}_s^* \Xi_c$, and $\bar{D}_s \Xi_c'$ in the ${}^2S_{1/2}$ wave. Another four channels in the ${}^2S_{1/2}$ wave are also minor effects on the $P_{c\bar{c}s s}(4504)$: $\bar{D}^* \Omega_c$, $\bar{D}^* \Omega_c^*$, $\bar{D}_s^* \Xi_c'$, and $\bar{D}_s^* \Xi_c''$ in the order of the magnitudes of the coupling strengths. Since the $P_{c\bar{c}s s}(4504)$ is located below the $\bar{D}_s \Xi_c'$ threshold, we expect that the $\bar{D}_s \Xi_c'$ governs the formation of the $P_{c\bar{c}s s}(4504)$. Interestingly, however, the $\bar{D} \Omega_c$ channel is the most dominant one. Had we turned off the contribution of this channel, the $P_{c\bar{c}s s}(4504)$ resonance would have disappeared, leaving only the enhancement in the $\bar{D}_s \Xi_c'$ threshold. On the other hand, even though we remove the $\bar{D}_s \Xi_c'$ channel, the $P_{c\bar{c}s s}(4504)$ survives. It indicates that it is essential to consider the $\bar{D} \Omega_c$ channel for the $P_{c\bar{c}s s}(4504)$. We have observed a similar situation in the $h_1(1385)$ meson resonance [39]. Finally, we want to mention that the D -wave contribution is tiny.

The pole position of the third resonance with $J^P = 1/2^-$ is given by $M_{P_{c\bar{c}s s}} - i\Gamma/2 = (4703.7 - i10.6)$ MeV in the complex plane. Its width is the largest among the $P_{c\bar{c}s s}$'s with negative parity. It is positioned below the $\bar{D}^* \Omega_c$ threshold. The $\bar{D}^* \Omega_c$ channel naturally provides the largest contribution to form the $P_{c\bar{c}s s}(4704)$ resonance. The $\bar{D}_s^* \Xi_c''$ gives the next largest contribution. As observed in Table II, the channels below the $\bar{D}^* \Omega_c$ threshold, i.e., the $\bar{D}_s^* \Xi_c' ({}^2S_{1/2})$, $\bar{D}_s \Xi_c' ({}^2S_{1/2})$, $\bar{D}_s^* \Xi_c ({}^2S_{1/2})$, and $\bar{D}_s \Xi_c ({}^4D_{1/2})$ have non-negligible values of the coupling strengths. This means that the $P_{c\bar{c}s s}(4704)$ can decay into the corresponding states, which is the reason for the relatively large width

TABLE II. Coupling strengths of the five $P_{c\bar{c}s s}$'s with $J^P = 1/2^-, 3/2^-,$ and $5/2^-$.

J^P	$P_{c\bar{c}s s}(4437)$	$P_{c\bar{c}s s}(4504)$	$P_{c\bar{c}s s}(4704)$	$P_{c\bar{c}s s}(4541)$	$P_{c\bar{c}s s}(4757)$
$\sqrt{s_R}$ [MeV]	4437.2 - $i0.002$	4504.1 - $i0.2$	4703.7 - $i10.6$	4541.3 - $i0.04$	4756.5 - $i1.7$
$g_{J/\psi\Xi}(^2S_J)$	0.10 + $i0.00$	0.29 + $i0.02$	0.03 + $i0.11$	-	-
$g_{J/\psi\Xi}(^2D_J)$	-	-	-	0.01 - $i0.00$	0.01 + $i0.00$
$g_{J/\psi\Xi}(^4S_J)$	-	-	-	0.27 + $i0.00$	-
$g_{J/\psi\Xi}(^4D_J)$	0.00 + $i0.00$	0.01 - $i0.00$	0.01 + $i0.02$	0.04 + $i0.00$	0.02 + $i0.00$
$g_{\bar{D}_s\Xi_c}(^2S_J)$	4.60 + $i0.01$	-0.03 + $i0.67$	0.85 + $i0.44$	-	-
$g_{\bar{D}_s\Xi_c}(^2D_J)$	-	-	-	0.03 + $i0.00$	-0.24 - $i0.17$
$g_{\bar{D}_s\Xi'_c}(^2S_J)$	0.17 + $i0.00$	11.72 - $i0.01$	-2.70 - $i0.58$	-	-
$g_{\bar{D}_s\Xi'_c}(^2D_J)$	-	-	-	0.00 + $i0.00$	-0.21 - $i0.15$
$g_{\bar{D}\Omega_c}(^2S_J)$	-0.23 - $i0.00$	-15.86 + $i0.02$	0.08 - $i2.24$	-	-
$g_{\bar{D}\Omega_c}(^2D_J)$	-	-	-	-0.00 - $i0.00$	0.95 + $i0.25$
$g_{\bar{D}_s^*\Xi_c}(^2S_J)$	-0.47 - $i0.00$	-13.90 - $i0.06$	-2.06 - $i1.87$	-	-
$g_{\bar{D}_s^*\Xi_c}(^2D_J)$	-	-	-	0.04 + $i0.00$	-0.00 - $i0.04$
$g_{\bar{D}_s^*\Xi_c}(^4S_J)$	-	-	-	-14.19 - $i0.01$	-
$g_{\bar{D}_s^*\Xi_c}(^4D_J)$	-0.01 - $i0.00$	0.12 + $i0.00$	-0.21 - $i0.18$	-0.04 - $i0.00$	0.08 + $i0.01$
$g_{\bar{D}_s\Xi_c^*}(^4S_J)$	-	-	-	-10.54 + $i0.00$	-
$g_{\bar{D}_s\Xi_c^*}(^4D_J)$	-0.00 - $i0.00$	0.05 + $i0.00$	1.18 + $i0.30$	-0.05 - $i0.00$	-0.28 - $i0.19$
$g_{\bar{D}\Omega_c^*}(^4S_J)$	-	-	-	14.69 + $i0.00$	-
$g_{\bar{D}\Omega_c^*}(^4D_J)$	0.00 + $i0.00$	-0.08 - $i0.00$	-0.09 + $i0.43$	0.08 + $i0.00$	1.52 + $i0.32$
$g_{\bar{D}_s^*\Xi'_c}(^2S_J)$	-2.41 - $i0.01$	-6.32 - $i0.52$	3.74 + $i0.89$	-	-
$g_{\bar{D}_s^*\Xi'_c}(^2D_J)$	-	-	-	-0.05 + $i0.00$	0.03 - $i0.04$
$g_{\bar{D}_s^*\Xi'_c}(^4S_J)$	-	-	-	4.50 - $i0.00$	-
$g_{\bar{D}_s^*\Xi'_c}(^4D_J)$	-0.07 - $i0.00$	0.13 + $i0.01$	0.43 - $i0.31$	0.05 - $i0.00$	-0.11 - $i0.02$
$g_{\bar{D}^*\Omega_c}(^2S_J)$	3.48 + $i0.01$	9.07 + $i0.74$	10.48 + $i3.81$	-	-
$g_{\bar{D}^*\Omega_c}(^2D_J)$	-	-	-	0.09 - $i0.00$	-0.33 - $i0.01$
$g_{\bar{D}^*\Omega_c}(^4S_J)$	-	-	-	-6.44 + $i0.00$	-
$g_{\bar{D}^*\Omega_c}(^4D_J)$	0.11 + $i0.00$	-0.22 - $i0.02$	0.00 - $i0.01$	-0.09 + $i0.00$	0.46 + $i0.05$
$g_{\bar{D}_s^*\Xi_c^*}(^2S_J)$	-2.80 - $i0.01$	4.75 - $i0.63$	8.87 - $i0.52$	-	-
$g_{\bar{D}_s^*\Xi_c^*}(^2D_J)$	-	-	-	0.09 + $i0.00$	0.00 + $i0.00$
$g_{\bar{D}_s^*\Xi_c^*}(^4S_J)$	-	-	-	8.29 + $i0.00$	-
$g_{\bar{D}_s^*\Xi_c^*}(^4D_J)$	0.06 + $i0.00$	0.16 - $i0.01$	0.01 - $i0.01$	-0.13 - $i0.00$	-0.00 - $i0.00$
$g_{\bar{D}_s^*\Xi_c^*}(^6S_J)$	-	-	-	-	7.58 + $i2.43$
$g_{\bar{D}_s^*\Xi_c^*}(^6D_J)$	0.16 + $i0.00$	0.07 - $i0.03$	0.13 + $i0.03$	0.04 + $i0.00$	0.00 + $i0.00$
$g_{\bar{D}^*\Omega_c^*}(^2S_J)$	4.12 + $i0.01$	-6.96 + $i0.91$	0.95 - $i1.30$	-	-
$g_{\bar{D}^*\Omega_c^*}(^2D_J)$	-	-	-	-0.14 - $i0.00$	-0.01 - $i0.00$
$g_{\bar{D}^*\Omega_c^*}(^4S_J)$	-	-	-	-12.17 - $i0.00$	-
$g_{\bar{D}^*\Omega_c^*}(^4D_J)$	-0.10 - $i0.00$	-0.25 + $i0.02$	-0.03 - $i0.03$	0.22 + $i0.00$	0.01 + $i0.00$
$g_{\bar{D}^*\Omega_c^*}(^6S_J)$	-	-	-	-	-8.02 - $i1.88$
$g_{\bar{D}^*\Omega_c^*}(^6D_J)$	-0.26 - $i0.00$	-0.13 + $i0.05$	0.08 + $i0.03$	-0.09 - $i0.00$	-0.02 - $i0.01$

of the $P_{c\bar{c}s s}(4704)$.

The upper-left panel of Fig. 4 shows the $P_{c\bar{c}s s}(4541)$ resonance with the pole position $M_{P_{c\bar{c}s s}} - i\Gamma/2 = (4541.3 - i0.04)$ MeV. It lies below the $\bar{D}_s\Xi'_c$ threshold. It is of great interest to see that while the $\bar{D}_s\Xi'_c(^2D_{3/2})$ channel does not contribute to the $P_{c\bar{c}s s}(4541)$ resonance, seven different channels in $^4S_{3/2}$ wave above the $\bar{D}_s\Xi'_c$ threshold contribute to it. The most dominant one comes from the $\bar{D}\Omega_c^*$ channel, and the next one, which is almost the same magnitude but has the different sign, arises from the $\bar{D}_s^*\Xi_c$. Its small width can be understood as follows: the $P_{c\bar{c}s s}(4541)$ cannot decay into the S -wave because of the conservation of the total angular momentum, it can only decay into meson-baryon states in D -wave below the $\bar{D}_s\Xi'_c$ threshold. This orbital excitation is physically not favorable, as shown in Table II. Note that it can also decay into the $J/\psi\Xi$ state in $^4S_{3/2}$ -wave, though the coupling strength is small. Finally, we want to mention that there is a cusp structure just below the $\bar{D}_s^*\Xi'_c$ threshold.

In the lower panel of Fig. 4, we draw the partial-wave cross section with $J^P = 5/2^-$, which illustrates a single resonance below the $\bar{D}_s^*\Xi'_c$ threshold. Its pole position is given by $M_{P_{c\bar{c}s s}} - i\Gamma/2 = (4756.5 - i1.7)$ MeV. The $\bar{D}^*\Omega_c^*(^6S_{5/2})$ channel yields the most dominant contribution. The next dominant one comes from the $\bar{D}_s^*\Xi_c^*(^6S_{5/2})$ one. Again, the small width of the $P_{c\bar{c}s s}(4757)$ can be understood from the fact that it cannot decay into lower S -wave

meson-baryon states.

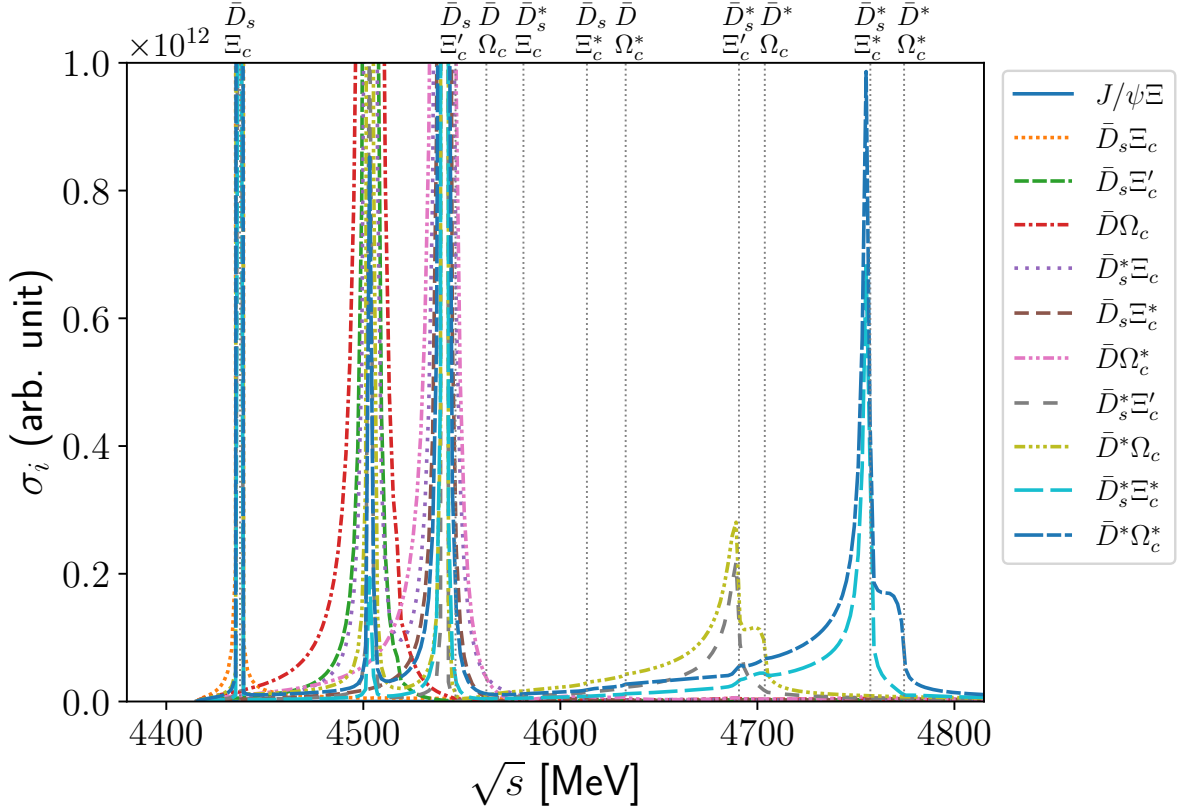


FIG. 5. Results for the total cross sections for elastic scattering as functions of the CM energy.

Figure 5 shows the results for the total cross sections of meson-baryon elastic scattering. While we seemingly observe the five pentaquark resonances discussed above, it depends on which scattering we consider. For example, we can see $P_{c\bar{c}s s}(4757)$ resonance with $J^P = 5/2^-$ only in the $\bar{D}_s^* \Xi_c^*$ and $\bar{D}^* \Omega_c^*$ scattering processes. As for the $P_{c\bar{c}s s}(4704)$ with $1/2^-$, we find it only in $\bar{D}_s^* \Xi'_c$ and $\bar{D}^* \Omega_c$ processes. The reason can be easily found by scrutinizing the coupling strengths listed in Table II. Note that we do not see any resonance signal in $J/\psi \Xi$ scattering. We find similar features in the $J/\psi N$ and $J/\psi \Lambda$ interactions [17, 18].

B. Positive parity

A significant feature of the current off-shell coupled channel formalism is that it also predicts the positive-parity pentaquark states coming from the P -wave contributions, as already examined in the production mechanism of the $P_{c\bar{c}}$ and $P_{c\bar{c}s}$ pentaquark states [17, 18]. Similarly, we also observe three double-strangeness hidden-charm resonances with positive parity. Figure 5 depicts the results for the $i \rightarrow J/\psi \Xi$ transition partial-wave cross sections with positive parity. In Table III, we list the results for the coupling strengths of the positive-parity $P_{c\bar{c}s s}$ pentaquark resonances to the channels involved. In the upper-left panel of Fig. 5, we observe a broad resonant structure, of which the pole position is at $(4665.6 - i57.8)$ MeV. It is located between the $\bar{D} \Omega_c^*$ and $\bar{D}_s^* \Xi'_c$ thresholds. In Table III, we find that four different channels, i.e., $\bar{D} \Omega_c^*(^4P_{1/2})$, $\bar{D}_s^* \Xi_c^*(^4P_{1/2})$, $\bar{D} \Omega_c(^2P_{1/2})$, and $\bar{D}_s^* \Xi'_c(^2P_{1/2})$ channels mainly contribute to form the $P_{c\bar{c}s s}(4666)$ resonance with $J^P = 1/2^+$. The pole position of the second resonance $P_{c\bar{c}s s}(4781)$ is obtained to be $(4781.1 - i25.7)$ MeV. Interestingly, many different channels contribute to it, as shown in Table III. The third resonance $P_{c\bar{c}s s}(4712)$ with $J^P = 3/2^+$ can be seen in the upper-right panel of Fig. 6, which is located at $(4712.3 - i30.8)$ MeV. The three different channels primarily govern the production of the $P_{c\bar{c}s s}(4712)$. There is no pentaquark resonance with $J^P = 5/2^+$ as depicted in the lower panel of Fig. 6, since only the $\bar{D}_s^* \Xi_c$ channel is large, whereas all other channels are suppressed.

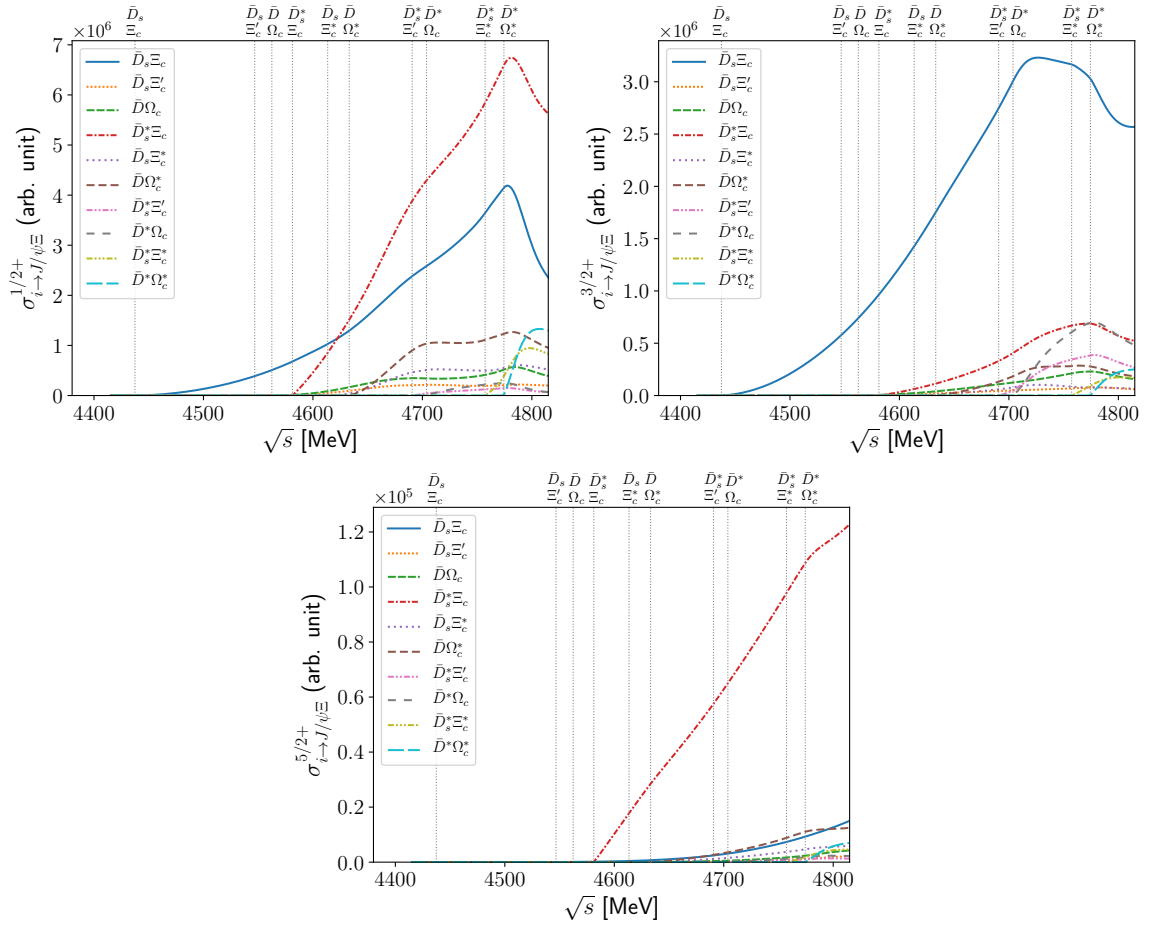


FIG. 6. Center-of-mass energy dependence of partial-wave total cross sections for positive-parity states ($J = 1/2, 3/2, 5/2$) corresponding to the spin-parity quantum numbers of $P_{c\bar{c}s}s$.

C. Uncertainties of the cutoff masses

Since there are no experimental data on the double-strangeness hidden-charm pentaquarks, we have no experimental guideline to fix the cutoff masses. Thus, we choose the reduced cutoff mass to be $\Lambda_0 = \Lambda - m = 700$ MeV, as in the previous studies [17, 18]. We examine the uncertainties that are caused by this value. Table IV demonstrates how the pole positions of the pentaquark resonances are shifted as Λ_0 is varied by 10%. When Λ_0 is increased, the masses of the pentaquark states with negative parity decrease whereas their widths are enlarged. On the other hand, when Λ_0 is decreased by 10%, the results are changed to the opposite direction. Moreover, $P_{c\bar{c}s}s(4437)$, $P_{c\bar{c}s}s(4704)$ and $P_{c\bar{c}s}s(4757)$ resonances are reduced to the cusp structures. The reason lies in the fact that by employing values of the cutoff masses softer than 700 MeV, the overall transition amplitudes are more suppressed. However, the masses of those with positive parity are slightly changed as Λ_0 is varied, whereas their widths are altered by about 20-30%. Future experimental data will clarify these uncertainties.

IV. SUMMARY AND CONCLUSION

In this work, we have investigated the possible existence of double-strangeness hidden-charm pentaquark states, denoted as $P_{c\bar{c}s}s$, using an off-shell coupled-channel formalism. We constructed eleven meson-baryon channels with total strangeness $S = -2$, combining charmed mesons and singly charmed baryons. The interaction kernel was derived from an effective Lagrangian that respects heavy-quark spin symmetry, hidden local symmetry, and flavor SU(3) symmetry. The coupled-channel scattering equations were solved in a partial-wave basis using the Blankenbecler-Sugar reduction scheme. We found five $P_{c\bar{c}s}s$ resonances with negative parity. Among them, three states have spin-parity $J^P = 1/2^-$, one has $J^P = 3/2^-$, and one has $J^P = 5/2^-$. All of these negative-parity states are

TABLE III. Coupling strengths of $P_{c\bar{c}s s}$'s with $J^P = 1/2^+$ and $3/2^+$.

J^P		$1/2^+$		$3/2^+$
$\sqrt{s_R}[\text{MeV}]$	4665.6 – $i57.8$		4781.1 – $i25.7$	4712.3 – $i30.8$
$g_{J/\psi\Xi}(^2P_J)$	0.03 – $i0.03$		0.16 – $i0.03$	0.02 – $i0.03$
$g_{J/\psi\Xi}(^4P_J)$	0.24 – $i0.28$		0.28 – $i0.07$	0.05 – $i0.04$
$g_{J/\psi\Xi}(^4F_J)$	–		–	0.00 – $i0.00$
$g_{\bar{D}_s\Xi_c}(^2P_J)$	0.06 – $i1.06$		–1.41 + $i0.45$	1.06 – $i0.84$
$g_{\bar{D}_s\Xi'_c}(^2P_J)$	2.01 – $i0.45$		0.55 + $i0.45$	–0.07 + $i0.28$
$g_{\bar{D}\Omega_c}(^2P_J)$	–2.85 + $i0.56$		–1.02 – $i0.64$	0.09 – $i0.30$
$g_{\bar{D}_s^*\Xi_c}(^2P_J)$	–0.23 + $i2.73$		–1.31 + $i0.95$	0.40 – $i0.76$
$g_{\bar{D}_s^*\Xi_c}(^4P_J)$	–0.05 + $i3.41$		–0.78 + $i0.94$	–0.25 + $i1.45$
$g_{\bar{D}_s^*\Xi_c}(^4F_J)$	–		–	–0.14 – $i0.01$
$g_{\bar{D}_s\Xi_c^*}(^4P_J)$	–3.00 + $i4.07$		–0.56 + $i0.10$	–1.25 + $i0.27$
$g_{\bar{D}_s\Xi_c^*}(^4F_J)$	–		–	0.22 – $i0.34$
$g_{\bar{D}\Omega_c^*}(^4P_J)$	3.15 – $i5.87$		0.85 + $i0.11$	2.04 – $i0.44$
$g_{\bar{D}\Omega_c^*}(^4F_J)$	–		–	–0.29 + $i0.26$
$g_{\bar{D}_s^*\Xi'_c}(^2P_J)$	0.00 + $i0.00$		–0.96 + $i0.86$	–0.54 + $i2.70$
$g_{\bar{D}_s^*\Xi'_c}(^4P_J)$	0.00 + $i0.00$		–0.19 + $i0.23$	2.65 – $i3.97$
$g_{\bar{D}_s^*\Xi'_c}(^4F_J)$	–		–	–0.04 + $i0.07$
$g_{\bar{D}^*\Omega_c}(^2P_J)$	0.00 + $i0.00$		1.37 – $i1.00$	0.48 – $i3.39$
$g_{\bar{D}^*\Omega_c}(^4P_J)$	0.00 + $i0.00$		0.29 – $i0.48$	–2.94 + $i5.09$
$g_{\bar{D}^*\Omega_c}(^4F_J)$	–		–	0.01 – $i0.06$
$g_{\bar{D}_s^*\Xi_c^*}(^2P_J)$	0.00 + $i0.00$		1.95 – $i3.33$	0.00 + $i0.00$
$g_{\bar{D}_s^*\Xi_c^*}(^4P_J)$	0.00 + $i0.00$		1.43 – $i1.79$	0.00 + $i0.00$
$g_{\bar{D}_s^*\Xi_c^*}(^4F_J)$	–		–	0.00 + $i0.00$
$g_{\bar{D}_s^*\Xi_c^*}(^6P_J)$	–		–	0.00 + $i0.00$
$g_{\bar{D}_s^*\Xi_c^*}(^6F_J)$	0.00 + $i0.00$		0.01 – $i0.09$	0.00 + $i0.00$
$g_{\bar{D}^*\Omega_c^*}(^2P_J)$	0.00 + $i0.00$		–2.00 + $4.24i$	0.00 + $i0.00$
$g_{\bar{D}^*\Omega_c^*}(^4P_J)$	0.00 + $i0.00$		–1.79 + $i2.64$	0.00 + $i0.00$
$g_{\bar{D}^*\Omega_c^*}(^4F_J)$	–		–	0.00 + $i0.00$
$g_{\bar{D}^*\Omega_c^*}(^6P_J)$	–		–	0.00 + $i0.00$
$g_{\bar{D}^*\Omega_c^*}(^6F_J)$	0.00 + $i0.00$		0.02 + $i0.05$	0.00 + $i0.00$

TABLE IV. The change in pole position due to the change of $\Lambda_0 = \Lambda - m$. The pole position in MeV unit.

J^P	$\Delta\Lambda_0/\Lambda_0$		
	0%	–10%	+10%
$1/2^-$	4437.2 – $i0.002$	cusplike	4420.8 – $i0.01$
	4504.1 – $i0.2$	4531.5 – $i0.1$	4466.0 – $i0.3$
	4703.7 – $i10.6$	cusplike	4633.2 – $i4.0$
$3/2^-$	4541.3 – $i0.04$	4570.8 – $i0.02$	4323.77 – $i0.04$
$5/2^-$	4756.5 – $i1.7$	cusplike	4750.1 – $i3.2$
$1/2^+$	4665.6 – $i57.8$	4665.2 – $i70.6$	4662.8 – $i46.0$
	4781.1 – $i25.7$	4782.5 – $i33.0$	4777.9 – $i19.5$
$3/2^+$	4712.3 – $i30.8$	4708.6 – $i38.9$	4711.9 – $i22.4$

located below their respective thresholds and are dynamically generated. The dominant channels contributing to each resonance were identified through the analysis of their coupling strengths. The narrowest state is found near the $\bar{D}_s\Xi_c$ threshold, while broader states appear closer to higher thresholds such as $\bar{D}^*\Omega_c$. In addition, three positive-parity $P_{c\bar{c}s s}$ states are found: two with spin-parity $J^P = 1/2^+$ and one with $J^P = 3/2^+$. These states are located above the corresponding thresholds and exhibit substantial widths. Their coupling patterns indicate significant contributions from multiple meson–baryon channels, especially those involving P -wave interactions.

The theoretical uncertainties associated with the cutoff mass were also examined by varying the reduced cutoff parameter $\Lambda_0 = \Lambda - m$ by $\pm 10\%$. This variation resulted in modest shifts in pole positions and in some cases transformed resonances into cusp-like structures, but the overall spectrum and structure remained qualitatively stable. The present study provides theoretical predictions for the mass spectrum, widths, and dominant coupling channels

of the double-strangeness hidden-charm pentaquark states. These predictions may serve as useful input for future experimental searches in processes involving the $J/\psi\Xi$ final state. The triple-strangeness hidden-charm pentaquark states can also be studied within the same framework, which is under investigation.

ACKNOWLEDGMENTS

The present work was supported by the Young Scientist Training (YST) Program at the Asia Pacific Center for Theoretical Physics (APCTP) through the Science and Technology Promotion Fund and Lottery Fund of the Korean Government and also by the Korean Local Governments – Gyeongsangbuk-do Province and Pohang City (SC), the Basic Science Research Program through the National Research Foundation of Korea funded by the Korean government (Ministry of Education, Science and Technology, MEST), Grant-No. RS-2025-00513982 (HChK), and the PUTI Q1 Grant from University of Indonesia under contract No. NKB-441/UN2.RST/HKP.05.00/2024 (TM).

-
- [1] R. Aaij *et al.* (LHCb), Phys. Rev. Lett. **115**, 072001 (2015), arXiv:1507.03414 [hep-ex].
- [2] R. Aaij *et al.* (LHCb), Phys. Rev. Lett. **122**, 222001 (2019), arXiv:1904.03947 [hep-ex].
- [3] R. Aaij *et al.* (LHCb), Phys. Rev. Lett. **128**, 062001 (2022), arXiv:2108.04720 [hep-ex].
- [4] A. Esposito, A. Pilloni, and A. D. Polosa, Phys. Rept. **668**, 1 (2017), arXiv:1611.07920 [hep-ph].
- [5] H.-X. Chen, W. Chen, X. Liu, Y.-R. Liu, and S.-L. Zhu, Rept. Prog. Phys. **80**, 076201 (2017), arXiv:1609.08928 [hep-ph].
- [6] L. Meng, B. Wang, G.-J. Wang, and S.-L. Zhu, Phys. Rept. **1019**, 1 (2023), arXiv:2204.08716 [hep-ph].
- [7] H.-X. Chen, W. Chen, X. Liu, Y.-R. Liu, and S.-L. Zhu, Rept. Prog. Phys. **86**, 026201 (2023), arXiv:2204.02649 [hep-ph].
- [8] R. Aaij *et al.* (LHCb), Phys. Rev. Lett. **131**, 031901 (2023), arXiv:2210.10346 [hep-ex].
- [9] I. Adachi *et al.* (Belle, Belle II), (2025), arXiv:2502.09951 [hep-ex].
- [10] A. Hayrapetyan *et al.* (CMS), Eur. Phys. J. C **84**, 1062 (2024), arXiv:2401.16303 [hep-ex].
- [11] R. Aaij *et al.* (LHCb), (2025), arXiv:2501.12779 [hep-ex].
- [12] F.-L. Wang, R. Chen, and X. Liu, Phys. Rev. D **103**, 034014 (2021), arXiv:2011.14296 [hep-ph].
- [13] P. G. Ortega, D. R. Entem, and F. Fernandez, Phys. Lett. B **838**, 137747 (2023), arXiv:2210.04465 [hep-ph].
- [14] J. A. Marsé-Valera, V. K. Magas, and A. Ramos, Phys. Rev. Lett. **130**, 091903 (2023), arXiv:2210.02792 [hep-ph].
- [15] L. Roca, J. Song, and E. Oset, Phys. Rev. D **109**, 094005 (2024), arXiv:2403.08732 [hep-ph].
- [16] J. A. Marsé-Valera, V. K. Magas, and A. Ramos, Phys. Rev. D **111**, 054020 (2025), arXiv:2410.10682 [hep-ph].
- [17] S. Clymton, H.-C. Kim, and T. Mart, Phys. Rev. D **110**, 094014 (2024), arXiv:2408.04166 [hep-ph].
- [18] S. Clymton, H.-C. Kim, and T. Mart, (2025), arXiv:2504.07693 [hep-ph].
- [19] A. Ali *et al.* (GlueX), Phys. Rev. Lett. **123**, 072001 (2019), arXiv:1905.10811 [nucl-ex].
- [20] R. Blankenbecler and R. Sugar, Phys. Rev. **142**, 1051 (1966).
- [21] R. Aaron, R. D. Amado, and J. E. Young, Phys. Rev. **174**, 2022 (1968).
- [22] R. Casalbuoni, A. Deandrea, N. Di Bartolomeo, R. Gatto, F. Feruglio, and G. Nardulli, Phys. Rept. **281**, 145 (1997), arXiv:hep-ph/9605342.
- [23] C. Isola, M. Ladisa, G. Nardulli, and P. Santorelli, Phys. Rev. D **68**, 114001 (2003), arXiv:hep-ph/0307367.
- [24] K. Kawarabayashi and M. Suzuki, Phys. Rev. Lett. **16**, 255 (1966).
- [25] Riazuddin and Fayyazuddin, Phys. Rev. **147**, 1071 (1966).
- [26] W. A. Bardeen, E. J. Eichten, and C. T. Hill, Phys. Rev. D **68**, 054024 (2003), arXiv:hep-ph/0305049.
- [27] Y.-R. Liu and M. Oka, Phys. Rev. D **85**, 014015 (2012), arXiv:1103.4624 [hep-ph].
- [28] T.-M. Yan, H.-Y. Cheng, C.-Y. Cheung, G.-L. Lin, Y. C. Lin, and H.-L. Yu, Phys. Rev. D **46**, 1148 (1992), [Erratum: Phys.Rev.D 55, 5851 (1997)].
- [29] R. Chen, Z.-F. Sun, X. Liu, and S.-L. Zhu, Phys. Rev. D **100**, 011502 (2019), arXiv:1903.11013 [hep-ph].
- [30] X.-K. Dong, F.-K. Guo, and B.-S. Zou, Progr. Phys. **41**, 65 (2021), arXiv:2101.01021 [hep-ph].
- [31] R. Casalbuoni, A. Deandrea, N. Di Bartolomeo, R. Gatto, F. Feruglio, and G. Nardulli, Phys. Lett. B **309**, 163 (1993), arXiv:hep-ph/9304280.
- [32] P. Colangelo, F. De Fazio, and T. N. Pham, Phys. Rev. D **69**, 054023 (2004), arXiv:hep-ph/0310084.
- [33] Y. Shimizu and M. Harada, Phys. Rev. D **96**, 094012 (2017), arXiv:1708.04743 [hep-ph].
- [34] H.-C. Kim, J. W. Durso, and K. Holinde, Phys. Rev. C **49**, 2355 (1994).
- [35] J.-Y. Kim and H.-C. Kim, Phys. Rev. D **97**, 114009 (2018), arXiv:1803.04069 [hep-ph].
- [36] J.-Y. Kim, H.-C. Kim, G.-S. Yang, and M. Oka, Phys. Rev. D **103**, 074025 (2021), arXiv:2101.10653 [hep-ph].
- [37] M. I. Haftel and F. Tabakin, Nucl. Phys. A **158**, 1 (1970).
- [38] R. Machleidt, K. Holinde, and C. Elster, Phys. Rept. **149**, 1 (1987).
- [39] S. Clymton and H.-C. Kim, Phys. Rev. D **110**, 114002 (2024), arXiv:2409.02420 [hep-ph].